


## Article

# Luenberger-Sliding Mode Observer Based Backstepping Control for the SCR System in a Diesel Engine

Taixiong Zheng <sup>1,\*</sup> , Bin Yang <sup>1</sup>, Yongfu Li <sup>2</sup> and Ying Ma <sup>1</sup>

<sup>1</sup> School of Advanced Manufacturing, Chongqing University of Posts and Telecommunications, Chongqing 400065, China; yangbin@cqupt.edu.cn (B.Y.); maying@cqupt.edu.cn (Y.M.)

<sup>2</sup> School of Automation, Chongqing University of Posts and Telecommunications, Chongqing 400065, China; liyongfu@cqupt.edu.cn

\* Correspondence: zhengtx@cqupt.edu.cn; Tel.: +135-2753-0922

Received: 25 October 2019; Accepted: 7 November 2019; Published: 8 November 2019



**Abstract:** In order to keep the ammonia ( $\text{NH}_3$ ) slip of the downstream selective catalytic reduction (SCR) system at a low level and simultaneously achieve a high nitrogen oxide ( $\text{NO}_x$ ) conversion rate, a Luenberger-sliding mode observer based backstepping control method is proposed. Considering that the internal working condition of the catalyst cannot be measured by commercial sensors directly, a Luenberger-sliding mode observer is designed to estimate the ammonia concentration at the middle of the catalyst. In addition, based on the stepped distributed characteristic of the surface ammonia coverage ratio along the SCR axial direction, a backstepping control method is utilized for the SCR system, in which the SCR system is decomposed into two subsystems. Firstly, the Lyapunov function is designed to ensure the convergence of the downstream subsystem, and then the virtual control law is obtained. After that, taking the virtual control law as the tracking target of the upstream subsystem, the Lyapunov function of virtual control law is given. Finally, the actual control law of the whole closed loop system is acquired. Simulations under different conditions are conducted to investigate the effect of the proposed control method. In addition, comparisons with the traditional PID (Proportion Integration Differentiation) control are presented. Results show that the proposed method is much better than the PID control method in overshoot, setting time, and tracking error.

**Keywords:** Backstepping control; diesel engine; Luenberger-sliding mode observer; SCR system

## 1. Introduction

Diesel engines have attracted more and more attention in recent years due to their high economy, high power, and low CO and HC emissions [1–3]. However, owing to the special combustion process, a diesel engine produces much more nitrogen oxide ( $\text{NO}_x$ ) and particulate matter (PM), which is harmful to the environment and human health. Various regulations have been legislated against diesel engine  $\text{NO}_x$  and PM emissions. In order to meet stringent regulations, devices such as selective catalytic reduction (SCR) systems and diesel particle filters (DPF) are installed in post-processing systems to reduce emissions. SCR refers to the use of reducing agents to selectively react with  $\text{NO}_x$  in flue gas and generate non-toxic and pollution-free  $\text{N}_2$  and  $\text{H}_2\text{O}$  under the action of a catalyst. Generally, in SCR systems, 32.5% of aqueous urea solution is injected into the tail gas pipe of the engine; urea is then decomposed into ammonia, which reacts with  $\text{NO}_x$  to generate  $\text{N}_2$  and  $\text{H}_2\text{O}$ . However, excessive urea can lead to  $\text{NH}_3$  leakage in the tailpipe and increase the usage cost. On the other hand, insufficient  $\text{NH}_3$  injection will lead to low  $\text{NO}_x$  conversion and higher tail pipe  $\text{NO}_x$  emissions [3,4]. A great deal of research has been done to minimize  $\text{NO}_x$  emissions and limit  $\text{NH}_3$  leaks at the same time, in which

a promising method is to control the  $\text{NH}_3$  concentration and coverage of  $\text{NH}_3$  in the SCR catalyst at the optimum [5].  $\text{NH}_3$  coverage and the ammonia coverage ratio are defined in (1), where  $\Theta$  is  $\text{NH}_3$  storage capacity and  $M_{\text{NH}_3}$  is the amount of  $\text{NH}_3$  stored inside the SCR catalyst.

$$\theta_{\text{NH}_3} = \frac{M_{\text{NH}_3}}{\Theta} \quad (1)$$

Much research has been conducted into SCR control systems [4–6]. In general, the SCR control strategy can be divided into non-model-based [7,8] and model-based [9–17]. The non-model-based methods include the pulse spectrum-based blue jet control method [7] and the PID control method [8]. Although the non-model-based method is relatively mature, its performance in transient and low temperature conditions makes it increasingly difficult to meet stricter emission regulations due to the problems of time delay, system inertia, and sensor measurement error and system uncertainty. As emission regulations become more and more stringent, model-based methods, such as predictive control [9], are needed urgently. Simulation and test bench results show that, compared to the non-model-based method, the model-based control method has higher accuracy and better environmental adaptability.

It should be mentioned that the values of  $\text{NH}_3$  concentration and  $\text{NH}_3$  coverage of the catalyst is vital for the SCR control system. Unfortunately, it is inconvenient to measure  $\text{NH}_3$  coverage directly through commercial sensors. To address the problem, observer based methods are prospective and widely used. Reference [18] presents an observer for estimating the  $\text{NH}_3$  concentration of catalysts in SCR. The observer can be used for  $\text{NH}_3$  distribution control of the SCR catalyst and fault diagnosis of the diesel engine. Experiments show that the observer estimates converge to the sensor readings and can track the values well. However, the concentration cannot be estimated well in the first 1100 seconds. In [4], an approach by utilizing two post-selective-catalytic-reduction nitrogen oxide sensors with different ammonia cross-sensitivity factors is proposed to estimate the nitrogen oxide concentration, the ammonia concentration, and the ammonia surface coverage ratio. Experimental results show that the proposed method can be useful in reducing the cost of SCR diagnosis,  $\text{NH}_3$  coverage estimation, and advanced SCR controls. In addition, an extended Kalman filter [19] can also be utilized to estimate the  $\text{NO}_x$  sensor cross-sensitivity to ammonia. It is noteworthy that the performance of an urea-SCR system may be related to the  $\text{NH}_3/\text{NO}_x$  ratio and the  $\text{NO}/\text{NO}_2$  ratio. Studies show that the ratio of  $\text{NO}$  to  $\text{NO}_2$  varies with the reduction rate and conversion efficiency of  $\text{NO}_x$  [1]. A sliding mode observer is widely used in system state estimation because of its strong robustness [20–23]. S. Hasan [24] introduced the Luenberger term into the design of the sliding mode observer, which not only improved the robustness of the observer, but also improved the speed of parameter estimation. Based on the above analysis, a Luenberger sliding mode observer is designed to estimate the state of the two-cell SCR catalyst.

Backstepping control is mainly used to deal with robust control systems with nonlinear and parametric uncertainties [25,26]. SCR is a typical nonlinear system with uncertain parameters, which is very suitable for backstepping control. Thus, in [27], the backstepping control is used successfully, but the unmeasurable problem of  $\text{NH}_3$  concentration is not mentioned.

In this paper, considering the advantages of the Luenberger-sliding mode observer [24] and backstepping control [25,26], a Luenberger-sliding mode observer based backstepping control method is applied to a nonlinear SCR system. The aims of this work are to simultaneously minimize the  $\text{NO}_x$  emissions and limit the  $\text{NH}_3$  slip under a certain input and output constraint. A Luenberger-sliding mode observer is designed to estimate  $\text{NH}_3$  concentration and then, based on the Lyapunov stability analysis and the stepped distributed characteristic of the surface  $\text{NH}_3$  coverage ratio along the SCR axial direction, a backstepping control method is designed for SCR system adblue dosing. After that, the stability analysis of the proposed control strategy is described. The proposed approach is validated through computer simulations that are compared with the traditional PID control. Simulation results show that the system controlled by the proposed method has promising performance in overshoot, setting time, and tracking error.

## 2. Selective Catalytic Reduction System

### 2.1. SCR System Operation Principles

Figure 1 is a schematic diagram of an SCR system, in which temperature, NO<sub>x</sub>, and NH<sub>3</sub> sensors are located upstream and downstream of the SCR catalyst. In order to monitor the status of the intermediate catalyst, NO<sub>x</sub> and NH<sub>3</sub> sensors are installed between two SCR batteries. Note that the inlet NO<sub>x</sub> measurement will not be contaminated by NH<sub>3</sub>, while the intermediate and downstream NO<sub>x</sub> sensors will be affected by the cross sensitivity of NH<sub>3</sub>. According to [27], the concentration of NO<sub>x</sub> is a combination of the NO<sub>x</sub> and NH<sub>3</sub> concentrations, as shown in (2):

$$C_{NO_x, mea} = C_{NO_x} + KC_{NH_3} \quad (2)$$

where  $C_{NO_x, mea}$  is the NO<sub>x</sub> sensor reading,  $C_{NO_x}$  is the true value of the NO<sub>x</sub> concentration,  $C_{NH_3}$  is the NH<sub>3</sub> concentration, and  $K$  denotes the cross-sensitivity factor. In this paper,  $K$  is considered to be a constant.

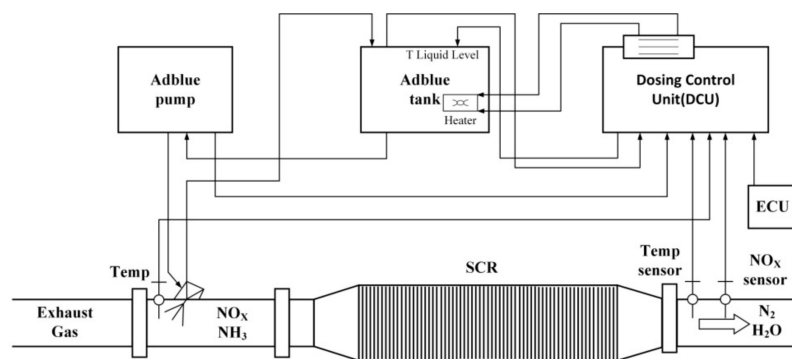
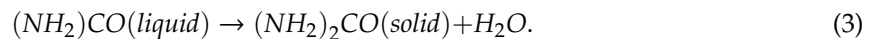


**Figure 1.** Schematic diagram of a selective catalytic reduction (SCR) system.

The reduction involves three processes. First, the urea solution sprayed into the upstream exhaust pipe is converted into NH<sub>3</sub>, which generally consists of three chemical reactions: Urea solution evaporation, urea decomposition, and isocyanic acid hydrolysis. The main chemical reactions are summarized as:

Aqueous urea solution evaporation:



Urea decomposition:



Isocyanic acid (HNCO) hydrolysis:



Then, the converted NH<sub>3</sub> is adsorbed on the surface of the catalyst matrix. Finally, the NH<sub>3</sub> reacts with NO<sub>x</sub> to form nitrogen molecules.

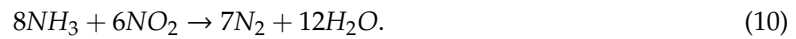
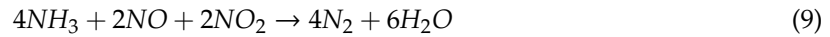
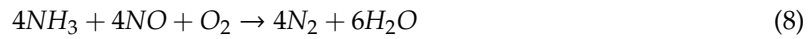
It should be noted that urea can be completely converted in the upstream tailpipe if the catalyst pool has a good geometric design and the exhaust has a suitable temperature [28]. Therefore, it is reasonable to assume that 100% of the urea aqueous solution is converted to gaseous NH<sub>3</sub> before the SCR catalyst unit.

The NH<sub>3</sub> adsorption and desorption reactions can be expressed as [29]:





where Z is the active substrate site of the SCR catalyst cell and  $ZNH_3$  represents  $NH_3$  adsorbed on the SCR substrate. The adsorbed  $NH_3$  is active enough to reduce the NOx in terms of the chemical reactions. The main NOx reduction process can be summarized as follows:



In some cases, when the gas temperature is quite high, the adsorbed  $NH_3$  can also be oxidized, as shown in (11):



## 2.2. SCR Dynamic Model and Analysis of Observability and Controllability

Assuming that the physical variables in the SCR catalyst unit are uniform, a SCR model is developed based on the above reaction. For convenience, the mass transfer and the surface phase concentration of species in the model are neglected. In this paper, the nonlinear model of the SCR model is expressed using the state-space form [29]:

$$\begin{bmatrix} \dot{C}_{NO} \\ \dot{\theta} \\ \dot{C}_{NH_3} \end{bmatrix} = \begin{bmatrix} -C_{NO}(\Theta r_{red}\theta + \frac{F}{V}) + r_{oxi}\Theta\theta \\ -\theta(r_{ads}C_{NH_3} + r_{des} + r_{red}C_{NO} + r_{oxi}) + r_{ads}C_{NH_3} \\ -C_{NH_3}[\Theta r_{ads}(1-\theta) + \frac{F}{V}] + \Theta r_{des}\theta \end{bmatrix} + \begin{bmatrix} 0 \\ 0 \\ \frac{F}{V} \end{bmatrix} C_{NH_3,in} + \begin{bmatrix} \frac{F}{V} \\ 0 \\ 0 \end{bmatrix} C_{NO,in} \quad (12)$$

where,  $C_{NO}$ ,  $C_{NH_3}$ ,  $C_{NO,in}$ , and  $C_{NH_3,in}$  are the concentrations of NO,  $NH_3$ , inlet NO, and inlet  $NH_3$ , respectively.  $r_{red}$ ,  $r_{ads}$ ,  $r_{des}$ , and  $r_{oxi}$  are standard reaction rate, adsorption rate, desorption rate, and oxidation rate, respectively.  $F$  is the exhaust flow rate and  $V$  is the SCR volume.  $\theta$  denotes the ammonia coverage ratio and  $R$  is the universal gas constant.

Let

$$x = [x_1 \ x_2 \ x_3]^T \quad (13)$$

where  $x_1 = C_{NO}$ ,  $x_2 = \theta$ ,  $x_3 = C_{NH_3}$ .

Linearize the nonlinear model with respect to operating points and obtain the linear state space equation:

$$\begin{cases} \dot{x} = Ax + Bu + Dd \\ y = Cx \end{cases} \quad (14)$$

where

$$A = \begin{bmatrix} A_{11} & A_{12} & A_{13} \\ A_{21} & A_{22} & A_{23} \\ A_{31} & A_{32} & A_{33} \end{bmatrix}, B = \begin{bmatrix} 0 \\ 0 \\ \frac{F}{V} \end{bmatrix}, D = \begin{bmatrix} \frac{F}{V} \\ 0 \\ 0 \end{bmatrix}, C = [0 \ 0 \ 1],$$

$$A_{11} = -\Theta r_{red}x_2 - \frac{F}{V}, A_{12} = -\Theta r_{red}x_1 + \Theta r_{oxi},$$

$$A_{13} = 0, A_{21} = -r_{red}x_2, A_{23} = r_{ads}(1-x_2),$$

$$A_{22} = -r_{ads}x_3 + r_{des} + r_{red}x_1 + r_{oxi}, A_{31} = 0,$$

$$A_{32} = \Theta r_{ads}x_3 + \Theta r_{des}, A_{33} = -\Theta r_{ads}(1-x_2) - \frac{F}{V}, u = C_{NH_3,in} \text{ is the inlet ammonia concentration,}$$

$d = C_{NO,in}$  is the inlet NO concentration.

The controllability grammian matrix takes the form:

$$Q_C = \begin{bmatrix} 0 & 0 & A_{12}A_{23} \\ 0 & A_{23} & (A_{22}A_{23} + A_{23}A_{33}) \\ 1 & A_{33} & (A_{23}A_{32} + A_{33}^2) \end{bmatrix}. \quad (15)$$

In most cases, the rank of the controllability grammian matrix is equal to 3. However, it may lose rank under certain operations:

- (1)  $A_{23} = 0$ ,  $\text{rank}(Q_C) = 1$ ; the  $\text{NH}_3$  coverage ratio and the  $\text{NO}_x$  concentration are uncontrollable. At that point, the  $\text{NH}_3$  coverage ratio reaches 100%. However, it will not happen in practice.
- (2)  $A_{12} = 0$ ,  $\text{rank}(Q_C) = 2$ ; the  $\text{NO}_x$  is uncontrollable. In the meantime,  $r_{oxi} > r_{red} \times C_{NO}$ , the reasonable working temperature, is below 600 °C. Therefore, the loss of controllability due to this condition is not expected operationally.

### 3. Observer Design and Stability Analysis

#### 3.1. Two-Cell SCR Catalyst Ammonia Concentration Observer Design

According to [8], ammonia storage in SCR catalysts varies along the axis of the catalysts. Moreover, the ammonia storage in the upstream and downstream of the SCR catalysts has a direct impact on the conversion of  $\text{NO}_x$  and the emission of  $\text{NH}_3$  in the tail gas. In order to express the internal state of the SCR catalytic converter more accurately, a two-cell SCR catalytic converter system is designed, shown in Figure 2 [18].

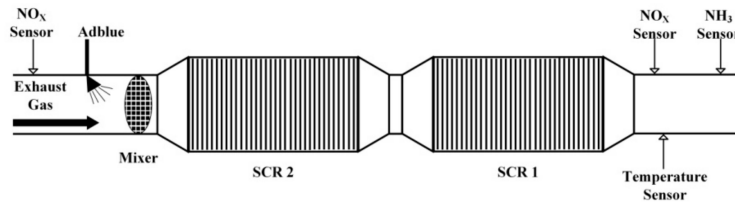


Figure 2. Two-cell SCR catalyst model.

Considering the  $\text{NH}_3$  concentration and  $\text{NH}_3$  coverage ratio, the dynamic model is presented as follows:

$$\dot{\theta}_1 = -\theta_1(r_{ads,1}C_{NH_3,1} + r_{des,1} + r_{red,1}C_{NO,1} + r_{oxi,1}) + r_{ads,1}C_{NH_3,1} \quad (16)$$

$$\dot{\theta}_2 = -\theta_2(r_{ads,2}C_{NH_3,2} + r_{des,2} + r_{red,2}C_{NO,2} + r_{oxi,2}) + r_{ads,2}C_{NH_3,2} \quad (17)$$

$$\dot{C}_{NH_3,1} = -C_{NH_3,1}[\Theta_1 r_{ads,1}(1 - \theta_1) + \frac{F_1}{V_1}] + \Theta_1 r_{des,1}\theta_1 + \frac{F_1}{V_1}C_{NH_3,2} \quad (18)$$

$$\dot{C}_{NH_3,2} = -C_{NH_3,2}[\Theta_2 r_{ads,2}(1 - \theta_2) + \frac{F_2}{V_2}] + \Theta_2 r_{des,2}\theta_2 + \frac{F_2}{V_2}C_{NH_3,in} \quad (19)$$

To estimate the  $\text{NH}_3$  coverage ratio, a Luenberger-sliding mode observer is proposed to observe the  $\text{NH}_3$  coverage ratio of the upstream cell [20]:

$$\dot{\hat{C}}_{NH_3,2} = -\hat{C}_{NH_3,2}[\Theta_2 r_{ads,2}(1 - \hat{\theta}_2) + \frac{F_2}{V_2}] + \Theta_2 r_{des,2}\hat{\theta}_2 + \frac{F_2}{V_2}C_{NH_3,in} + l_{2,2}(C_{NH_3,1} - \hat{C}_{NH_3,2}) + k_{2,2}\text{sgn}(C_{NH_3,1} - \hat{C}_{NH_3,2}) \quad (20)$$

where

$$\dot{\hat{\theta}}_2 = -\hat{\theta}_2(r_{ads,2}\hat{C}_{NH_3,2} + r_{des,2} + r_{red,2}\hat{C}_{NO,2} + r_{oxi,2}) + r_{ads,2}\hat{C}_{NH_3,2} + l_{1,2}(\hat{C}_{NH_3,2} - \hat{C}_{NH_3,1}) + k_{1,2}\text{sgn}(\hat{C}_{NH_3,2} - \hat{C}_{NH_3,1}) \quad (21)$$

$$\dot{\hat{\theta}}_1 = -\hat{\theta}_1(r_{ads,1}\hat{C}_{NH_3,1} + r_{des,1} + r_{red,1}C_{NO,1} + r_{oxi,1}) + r_{ads,1}\hat{C}_{NH_3,1} \quad (22)$$

$$\dot{\hat{C}}_{NH_3,1} = -\hat{C}_{NH_3,1}[\Theta_1 r_{ads,1}(1 - \hat{\theta}_1) + \frac{F_1}{V_1}] + \Theta_1 r_{des,1}\hat{\theta}_1 + \frac{F_1}{V_1}C_{NH_3,2} + l_{2,1}(C_{NH_3,1} - \hat{C}_{NH_3,1}) + k_{2,1}\text{sgn}(C_{NH_3,1} - \hat{C}_{NH_3,1}) \quad (23)$$

$$\dot{\hat{C}}_{NO,2} = -\hat{C}_{NO,2}(\Theta_2 r_{red,2}\hat{\theta}_2 + \frac{F_2}{V_2}) + r_{oxi,2}\Theta_2\hat{\theta}_2 + \frac{F_2}{V_2}C_{NO,in} \quad (24)$$

$$k_{1,2}, k_{2,1}, k_{2,2} > 0, 0 \leq \hat{\theta}_2, \hat{\theta}_1 \leq 1, 0 \leq \hat{C}_{NH_3,1} < 1, \hat{C}_{NH_3,2} \leq \hat{C}_{NH_3,max} < 1.$$

### 3.2. Observer Stability Analysis

As mentioned above, the  $\text{NH}_3$  coverage ratio is one of the important factors for the  $\text{NH}_3$  storage distribution control, and its estimation requires the  $\text{NH}_3$  concentration. The observability is demonstrated in the following [28]:

#### 3.2.1. Convergence Analysis of $\hat{\theta}_1$

First, select the Lyapunov function candidate as:

$$V_{\theta_1} = \frac{1}{2} \tilde{\theta}_1^2. \quad (25)$$

Then, the differentiate (25), gives:

$$\dot{V}_{\theta_1} = \tilde{\theta}_1 \dot{\tilde{\theta}}_1 = -\tilde{\theta}_1^2 (r_{\text{ads},1} \hat{C}_{\text{NH}_3,1} + r_{\text{des},1} + r_{\text{red},1} C_{\text{NO},1} + r_{\text{oxi},1}). \quad (26)$$

It is apparent that  $\dot{V}_{\theta_1} \leq 0$ , which means that  $\hat{\theta}_1$  converges to  $\theta_1$  within a finite period of time.

#### 3.2.2. Convergence Analysis of $\hat{C}_{\text{NH}_3,2}$

Convergence analysis of  $\hat{C}_{\text{NH}_3,2}$

$$\dot{\tilde{C}}_{\text{NH}_3,1} = \frac{F_1}{V_1} \tilde{C}_{\text{NH}_3,2} - l_{2,1} (\tilde{C}_{\text{NH}_3,1}) - k_{2,1} \text{sgn}(\tilde{C}_{\text{NH}_3,1}) \quad (27)$$

since  $0 \leq \tilde{C}_{\text{NH}_3,2} \leq C_{\text{NH}_3,\text{max}}$ , let  $k_{2,1} > \frac{F_{1,\text{max}}}{V_1} C_{\text{NH}_3,\text{max}}$ , then  $\hat{C}_{\text{NH}_3,2}$  can converges to  $C_{\text{NH}_3,2}$  in a finite period of time. Once the sliding mode is reached in the short term, there will be  $\dot{\tilde{C}}_{\text{NH}_3,1} = \tilde{C}_{\text{NH}_3,1} = 0$ . That means:

$$\frac{F_1}{V_1} \tilde{C}_{\text{NH}_3,2} = k_{2,1} \text{sgn}(\tilde{C}_{\text{NH}_3,1}) \quad (28)$$

$$\text{sgn}(\tilde{C}_{\text{NH}_3,2}) = \text{sgn}(\tilde{C}_{\text{NH}_3,1}). \quad (29)$$

Select the Lyapunov function candidate as:

$$V_{C_{\text{NH}_3,2}} = \frac{1}{2} \tilde{C}_{\text{NH}_3,2}^2. \quad (30)$$

Then, differentiate (31) gives:

$$\dot{V}_{C_{\text{NH}_3,2}} = \tilde{C}_{\text{NH}_3,2} \dot{\tilde{C}}_{\text{NH}_3,2} = -\tilde{C}_{\text{NH}_3,2} [-\tilde{C}_{\text{NH}_3,2} (\Theta_2 r_{\text{ads},2} + \frac{F_2}{V_2}) + C_{\text{NH}_3,2} \Theta_2 r_{\text{ads},2} - \hat{C}_{\text{NH}_3,2} \Theta_2 r_{\text{ads},2} \hat{\theta}_2 + \Theta_2 r_{\text{ads},2} \tilde{\theta}_2 - l_{2,2} (\tilde{C}_{\text{NH}_3,2}) - k_{2,2} \text{sgn}(\tilde{C}_{\text{NH}_3,2})] \quad (31)$$

Let  $k_{2,2} > \max |C_{\text{NH}_3,2} \Theta_2 r_{\text{ads},2} - \hat{C}_{\text{NH}_3,2} \Theta_2 r_{\text{ads},2} \hat{\theta}_2 + \Theta_2 r_{\text{ads},2} \tilde{\theta}_2|$ , then  $\dot{V}_{C_{\text{NH}_3,2}}$  is negative and definite, and  $\hat{C}_{\text{NH}_3,2}$  converges to  $C_{\text{NH}_3,2}$  in a finite period of time.

#### 3.2.3. Convergence Analysis of $\hat{\theta}_2$

Let  $\tilde{C}_{\text{NH}_3,2} = 0$  as a sliding surface; once the sliding mode is reached, there will be  $\dot{\tilde{C}}_{\text{NH}_3,2} = \tilde{C}_{\text{NH}_3,2} = 0$ . Select the Lyapunov function candidate as:

$$V_{\theta_2} = \frac{1}{2} \tilde{\theta}_2^2. \quad (32)$$

Then, differentiate (32) gives:

$$\dot{V}_{\theta_2} = \tilde{\theta}_2 \dot{\tilde{\theta}}_2 = \tilde{\theta}_2 [-\tilde{\theta}_2 (r_{des,2} + r_{red,2} \hat{C}_{NO,2} + r_{oxi,2}) + \hat{\theta}_2 r_{ads,2} \hat{C}_{NH_3,2} - \hat{\theta}_2 r_{ads,2} \hat{C}_{NH_3,2} + r_{ads,2} \tilde{C}_{NH_3,2} - l_{1,2} (\tilde{C}_{NH_3,2}) - k_{1,2} \text{sgn}(\tilde{C}_{NH_3,2})] \quad (33)$$

Let  $k_{1,2} > |C_{NH_3,2} r_{ads,2}|_{\max}$ , then  $\dot{V}_{\theta_2}$  is negative and definite, and  $\hat{\theta}_2$  can converge to  $\theta_2$  in a finite period of time.

#### 4. Backstepping Control Law Design

In order to keep  $NH_3$  leakage of the downstream SCR system at a low level and achieve a high  $NO_x$  conversion rate at the same time, the controller should keep downstream  $NH_3$  coverage below constraint  $\theta_1^*$  and control upstream  $NH_3$  coverage at the desired target,  $\theta_2^*$ . Based on the two-cell SCR system model, the dynamic equations are expressed as [18]:

$$\dot{x}_1 = F_1(x_1, x_3, T, C_{NO}) + G_1(x_1, x_3, T, C_{NO})x_3 \quad (34)$$

$$\dot{x}_2 = F_2(x_1, x_2, \Theta, T, F, V) + G_2(x_1, x_2, \Theta, T, F, V)x_4 \quad (35)$$

$$\dot{x}_3 = F_3(x_4, x_3, \Theta, T, F, V) + G_3(x_4, x_3, \Theta, T, F, V)u \quad (36)$$

$$\dot{x}_4 = F_4(x_3, x_4, T, C_{NO}) + G_4(x_3, x_4, T, C_{NO})x_4 \quad (37)$$

where

$$[x_1 \ x_2 \ x_3 \ x_4]^T = [\theta_1 \ C_{NH_3,1} \ \theta_2 \ C_{NH_3,2}]^T \quad (38)$$

$$[x_{1,\min} \ x_{2,\min} \ x_{3,\min} \ x_{4,\min}]^T \leq [x_1 \ x_2 \ x_3 \ x_4]^T \leq [x_{1,\max} \ x_{2,\max} \ x_{3,\max} \ x_{4,\max}]^T \quad (39)$$

$$G_1(\cdot) > 0, G_2(\cdot) > 0, G_3(\cdot) > 0, G_4(\cdot) > 0, F_1(\cdot) < 0, F_4(\cdot) < 0.$$

According to the backstepping theory, the control law is designed to let  $x_4$  approach  $\theta_2^*$  under the condition  $x_1 \leq \theta_1^*$ .

$$u = \frac{-G_2(x_2 - \xi_1) - G_4(x_4 - \theta_2^*) - K_3 \text{sign}(x_3 - \xi_2) - F_3 + \dot{\xi}_2}{G_3} \quad (40)$$

$$\xi_1 = -K_1 \frac{x_1 - \theta_1^*}{1 - x_1} \quad (41)$$

$$\xi_2 = \frac{-K_2(x_2 - \xi_1) - F_2 + \dot{\xi}_2 - K_0 G_1(x_1 - \theta_1^*)}{G_2} \quad (42)$$

$$K_1 = \frac{C}{2G_4(1 - \theta_1^*)} (\text{sign}((x_1 - \theta_1^*)(x_4 - \theta_2^*)) + 1), C > 0 \quad (43)$$

$$K_2 > \frac{|F_2|_{\max} + K_0 G_{1,\max}}{x_{2,\min}} \quad (44)$$

$$K_3 > G_{4,\max} |x_4 - \theta_2^*|_{\max} \quad (45)$$

$$\text{sign}(x) = \begin{cases} -1, & x < 0 \\ 0, & x = 0 \\ 1, & x > 0 \end{cases} \quad (46)$$

Stability of the backstepping is necessary for the controller design. For this system, two cases should be considered. One is  $x_1 > \theta_1^*$ ; at this time, the downstream ammonia coverage ratio is fairly high, and  $x_1$  can converge to  $\theta_1^*$ . Another is  $x_1 \leq \theta_1^*$ ; the constraint is satisfied, and  $x_4$  can converge to  $\theta_2^*$ .

#### 4.1. Stability Analysis of Case 1

(1) For Equation (34), the Lyapunov function candidate can be defined as:

$$V_1 = \frac{K_0}{2} \hat{x}_1^2 > 0 \quad (47)$$

where  $\hat{x} = x_1 - \theta_1^*$  and  $K_0 > 0$ , and taking the time derivative of  $V_1$  gives

$$\dot{V}_1 = K_0 \hat{x}_1 \dot{\hat{x}}_1 = K_0 \hat{x}_1 F_1 + K_0 \hat{x}_1 G_1 x_3. \quad (48)$$

Combining (34) with (38) obtains:

$$\dot{V}_1 = -K_0 \hat{x}_1 (\hat{x}_1 + \theta_1^*) (r_{des,1} + r_{red,1} C_{NO,1} + r_{oxi,i}) + K_0 r_{ads,1} \hat{x}_1 x_2 (1 - (\hat{x}_1 + \theta_1^*)) K_0 \hat{x}_1 F_1. \quad (49)$$

Select the virtual control input  $x_2$  as  $\xi_1$ . Combined, (40) and (43), gives

$$x_{2,vir} = \xi_1 = -K_1 \frac{x_1 - \theta_1^*}{1 - x_1} = \frac{C(x_1 - \theta_1^*)}{2G_4(1 - \theta_1^*)(1 - x_1)} (\text{sign}((x_1 - \theta_1^*)(x_4 - \theta_2^*)) + 1). \quad (50)$$

Then

$$\dot{V}_1 = -K_0 \hat{x}_1 (\hat{x}_1 + \theta_1^*) (r_{des,1} + r_{red,1} C_{NO,1} + r_{oxi,i}) - \frac{CK_0 \hat{x}_1^2 r_{ads,1}}{2G_4(1 - \theta_1^*)} (\text{sign}((x_1 - \theta_1^*)(x_4 - \theta_2^*)) + 1) \quad (51)$$

because  $\hat{x}_1 > 0$

$$\hat{x}_1 (\hat{x}_1 + \theta_1^*) (r_{des,1} + r_{red,1} C_{NO,1} + r_{oxi,i}) > \hat{x}_1^2 (r_{des,1} + r_{red,1} C_{NO,1} + r_{oxi,i}) > 0 \quad (52)$$

and

$$\frac{CK_0 \hat{x}_1^2 r_{ads,1}}{2G_4(1 - \theta_1^*)} (\text{sign}((x_1 - \theta_1^*)(x_4 - \theta_2^*)) + 1) \geq 0 \quad (53)$$

$$\dot{V}_1 \leq -K_0 \hat{x}_1 (\hat{x}_1 + \theta_1^*) (r_{des,1} + r_{red,1} C_{NO,1} + r_{oxi,i}) \leq -K_0 \hat{x}_1^2 (\hat{x}_1 + \theta_1^*) (r_{des,1} + r_{red,1} C_{NO,1} + r_{oxi,i}) = -Q_1 < 0 \quad (54)$$

where,  $Q_1$  is positive and definite. Therefore,  $x_1$  can converge to  $\theta_1^*$ .

(2) For Equation (35), in order to ensure that the real  $x_2$  can converge to the desired value,  $x_{2,tar}$ , with the action of  $\xi_2$ , the Lyapunov function candidate can be defined as:

$$V_2 = V_1 + \frac{1}{2} z_2^2 = \frac{K_0}{2} \hat{x}_1^2 + \frac{1}{2} z_2^2 \quad (55)$$

where

$$z_2 = x_2 - \xi_1. \quad (56)$$

Taking the time derivative of  $V_2$  gives:

$$\dot{V}_2 = K_0 \hat{x}_1 \dot{\hat{x}}_1 + z_2 \dot{z}_2. \quad (57)$$

Because  $x_2 = \xi_1 + z_2$ , according to (48) and (64), we can get:

$$\begin{aligned} \dot{V}_2 &\leq -K_0 \hat{x}_1^2 (\hat{x}_1 + \theta_1^*) (r_{des,1} + r_{red,1} C_{NO,1} + r_{oxi,i}) + K_0 \hat{x}_1 G_1 z_2 + z_2 (\dot{x}_2 - \dot{\xi}_1) \\ &= -Q_1 + z_2 (K_0 \hat{x}_1 G_1 + F_2 + G_2 x_3 - \dot{\xi}_1) \end{aligned} \quad (58)$$

Letting  $x_3 = \xi_2$ , as the virtual control signal, gets:

$$\dot{V}_2 \leq -K_0 \hat{x}_1^2 (\hat{x}_1 + \theta_1^*) (r_{des,1} + r_{red,1} C_{NO,1} + r_{oxi,i}) - K_2 x_2^2 = -Q_2 < 0 \quad (59)$$

where,  $Q_2$  is positive and definite. Therefore,  $x_2$  can converge to  $x_{2,tar}$ .

(3) For Equation (36), in order to ensure that  $x_3$  can converge to the desired value,  $x_{3,tar}$ , with the action of input signal  $u$ , the Lyapunov function candidate can be defined as:

$$V_3 = V_2 + \frac{1}{2} z_3^2 \quad (60)$$

where  $z_3 = x_3 - \xi_2$ . Analogously, according to (59), taking the time derivative of  $V_3$  gives:

$$\dot{V}_3 = \dot{V}_2 + z_3 \dot{z}_3 \leq -Q_2 + G_2 z_2 z_3 + z_3 (\dot{x}_3 - \dot{\xi}_2) = -Q_2 + z_3 (G_2 z_2 + F_3 + G_3 u - \dot{\xi}_2). \quad (61)$$

Based on (40) and (61), it can be achieved by:

$$\dot{V}_3 \leq -Q_2 - z_3 (K_3 \text{sign}(z_3) + g_4 (x_4 - \theta_2^*)) = -Q_3. \quad (62)$$

Because  $K_3 > g_{4,\max} |x_4 - \theta_2^*|_{\max}$ ,  $\dot{V}_3 < 0$ ,  $x_3$  can converge to  $x_{3,tar}$ .

According to the above mentioned analysis, based on the Lyapunov functions (47), (55), (60), and the control law (39),  $x_1$ ,  $x_2$ , and  $x_3$  can converge to the desired value, respectively.

#### 4.2. Stability Analysis of Case 2

In this case, the  $\text{NH}_3$  coverage ratio of the downstream SCR system should be lower than the value  $x_{2,tar}$ , therefore, the Lyapunov function is design to prove that  $x_4$  can converge to  $\theta_2^*$  with the action of  $\xi_2$ .

(1) For Equation (34), select  $\xi_2$  as the virtual control input of  $x_3$ ; the Lyapunov function candidate can be defined as:

$$V_4 = \frac{1}{2} \hat{x}_4^2 \quad (63)$$

where  $\hat{x}_4 = x_4 - \theta_2^*$ .

Taking the time derivative of  $V_4$ , gives:

$$\dot{V}_4 = \hat{x}_4 \dot{\hat{x}}_4 = \hat{x}_4 (F_4 + G_4 x_3). \quad (64)$$

Let  $x_{3,tar} = \xi_2$ , then:

$$\dot{V}_4 = \hat{x}_4 \dot{\hat{x}}_4 = \hat{x}_4 (f_4 + g_4 \xi_2) = \hat{x}_4 (f_4 + \frac{g_4}{g_2} (-K_2 (x_2 - \xi_1) - f_2 + \dot{\xi}_2 - K_0 g_1 (x_1 - \theta_1^*))). \quad (65)$$

At this moment, there are two different conditions needing consideration.

If  $x_1 < \theta_1^*$  and  $x_4 \geq \theta_2^*$ , then  $\text{sign}((x_1 - \theta_1^*)(x_4 - \theta_2^*) + 1) = 0$ ,  $K_1 = 0$ , and  $\xi_1 = \dot{\xi}_1 = 0$ .  $\dot{V}_4$  can be written as:

$$\dot{V}_4 = \hat{x}_4 (f_4 - \frac{g_4}{g_2} (K_2 x_2 + f_2 + K_0 g_1 (x_1 - \theta_1^*))). \quad (66)$$

Based on (44):

$$\begin{aligned} \dot{V}_4 &\leq \hat{x}_4 (f_{4,\max} - \frac{g_{4,\max}}{g_{2,\max}} (K_2 x_{2,\min} + f_2 - K_0 g_1)) \\ &\leq \hat{x}_4 (f_{4,\max} - \frac{g_{4,\max}}{g_{2,\max}} (|f_2|_{\max} + K_0 g_{1,\min} + f_2 + K_0 g_1)) < 0 \end{aligned} \quad (67)$$

Since  $\dot{V}_4$  is negative and definite,  $x_4$  can converge to  $\theta_2^*$ .

If  $x_1 < \theta_1^*$  and  $x_4 < \theta_2^*$ , in order that  $\dot{V}_4$  is negative and definite, according to (65), it can be achieved by:

$$F_4 + G_4 \xi_2 > 0. \quad (68)$$

Combined, (40), (41), and (43), obtain:

$$F_4 + G_4 \xi_2 = F_4 + \frac{G_4}{G_2} \left[ -K_2(x_2 + K_1 \frac{x_1 - \theta_1^*}{1 - x_1}) - F_2 - K_1 \frac{(F_1 - G_1 x_2)(1 - \theta_1^*)}{(1 - x_1)^2} - K_0 G_1 (x_1 - \theta_1^*) \right]. \quad (69)$$

Since  $x_1 < \theta_1^*$  and  $x_4 < \theta_2^*$ , (68) can be achieved if the following condition is satisfied:

$$x_1 - \theta_1^* < \frac{G_2(1 - x_1)(1 - \theta_1^*)}{K_2 C + G_1 G_4 K_0(1 - x_1)(1 - \theta_1^*)} \left[ F_4 - \frac{K_2 G_4 x_2}{G_2} - \frac{G_4 F_2}{G_2} - \frac{C(F_1 + G_1 x_2)(1 - \theta_1^*)}{G_2(1 - x_1)^2} \right] = \omega. \quad (70)$$

If  $\omega \geq 0$ ,  $\hat{x}_1$  can converge to zero. If  $\omega < 0$  and  $C$  and  $K_2$  are large enough,  $\omega$  can be very close to zero, which means that  $x_4$  can converge to  $\theta_2^*$  when  $x_1 < \theta_1^* - |\omega|$ .

(2) For Equation (35), the Lyapunov function candidate can be defined as:

$$V_5 = V_4 + \frac{1}{2} z_3^2. \quad (71)$$

According to (65) and (39), it can be achieved by:

$$\begin{aligned} \dot{V}_5 &= \dot{V}_4 + z_3 \dot{z}_3 \leq G_4 z_3 \hat{x}_4 + z_3 (\dot{x}_3 - \dot{\xi}_2) \\ &= z_3 (\hat{x}_4 G_4 + F_3 + G_3 u - \dot{\xi}_2) = -z_3 (K_3 \text{sign}(z_3) + G_2 z_2) \end{aligned} \quad (72)$$

Based on (45),  $\dot{V}_5$  is negative,  $x_3$  can converge to  $\xi_2$ , and  $x_4$  can converge to  $\theta_2^*$ .

## 5. Experiment Results and Analysis

Several studies have reported that the combination of DOC (Diesel Oxidation Catalyst), DPF, and SCR has become one of the most common post-processing applications in heavy diesel engines, which can handle PM and NO<sub>x</sub> simultaneously [30–32]. Normally, DOC, installed upstream of the SCR catalysts, is utilized to convert part of NO into NO<sub>2</sub>. At the same time, DPF, installed between the DOC and the SCR, is used for reducing PM emissions. Figure 3 shows a schematic diagram of a SCR after-treatment system. The detail parameters of the parts are listed in Tables 1–4.

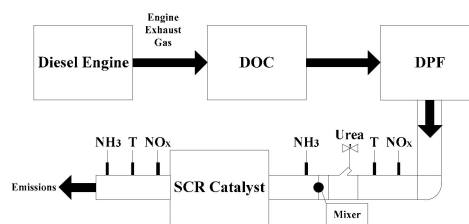


Figure 3. Schematic diagram of SCR after-treatment system for simulation.

Table 1. The detail parameters of the Engine.

Item	Quantity
Engine type	4-cylinder
Bore (mm)	100
Stroke (mm)	110
Connecting rod length (mm)	152
Compression ratio	18
Engine displacement (liter)	3

**Table 2.** Configuration parameters of SCR in GT power.

Item	Quantity
Cell density (1/inch <sup>2</sup> )	400
Length (mm)	250
Diameter (mm)	25
Active surface site density (mole/m <sup>3</sup> )	125

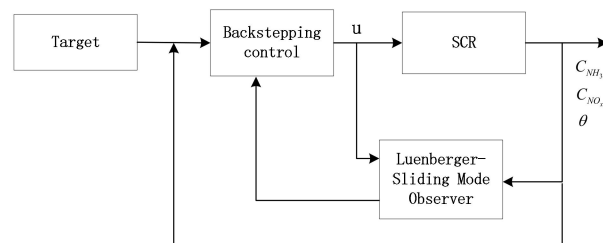
**Table 3.** Configuration parameters of DOC in GT-power.

Item	Quantity
Channel geometry	square
Front area (mm <sup>2</sup> )	20000
Cell density (1/inch <sup>2</sup> )	400
Length (mm)	150

**Table 4.** Configuration parameters of DPF in GT-power.

Item	Quantity
Trap diameter (mm)	130
Filter wall thickness (inch)	0.014
Channel length (mm)	260
Inlet cell density (1/inch <sup>2</sup> )	95

According to the proposed algorithm, the schematic diagram of the control system is designed as shown in Figure 4. In the system, the NH<sub>3</sub> concentration is estimated by the Luenberger-sliding mode observer and used as the input of the backstepping control. After that, the SCR is controlled by the controller.

**Figure 4.** Schematic diagram of the control system.

### 5.1. Experiment Validation of Luenberger-Sliding Mode Observer

In this section, the effectiveness of the observer will be validated first. Because the main reactions on the catalyst are standard reactions and fast reactions, as shown in (8) and (9), the simple model-based controller is targeting a molar ratio of NH<sub>3</sub>/NO<sub>x</sub> of 1/1 in order to suppress NH<sub>3</sub> leakage. The observer result of the mid-catalyst NH<sub>3</sub> concentration at three different NO<sub>2</sub>/NO ratios and different temperatures are shown in Figures 5–13.

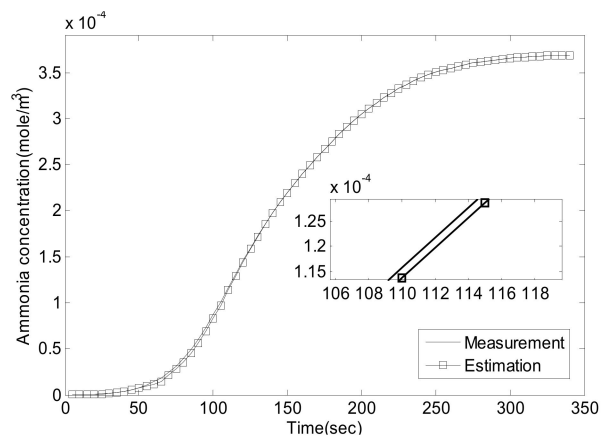


Figure 5.  $\text{NO}_2/\text{NO} = 0/1$ , 30 °C, comparison of  $C_{\text{NH}_3,2}$ .

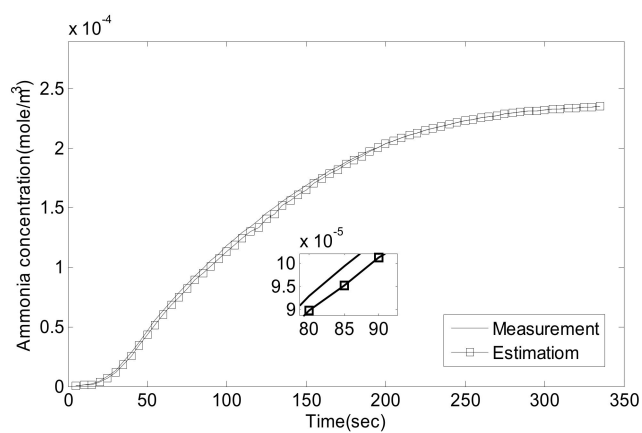


Figure 6.  $\text{NO}_2/\text{NO} = 0/1$ , 350 °C, comparison of  $C_{\text{NH}_3,2}$ .

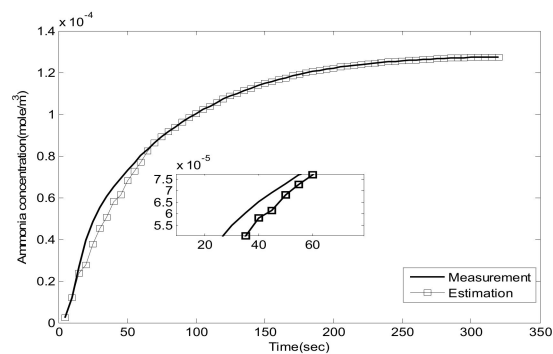


Figure 7.  $\text{NO}_2/\text{NO} = 0/1$ , 400 °C, comparison of  $C_{\text{NH}_3,2}$ .

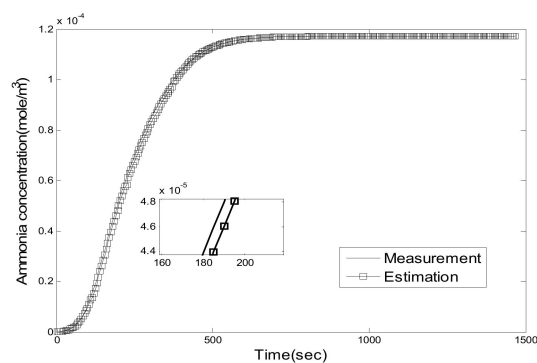


Figure 8.  $\text{NO}_2/\text{NO} = 1/2$ , 300 °C, comparison of  $C_{\text{NH}_3,2}$ .

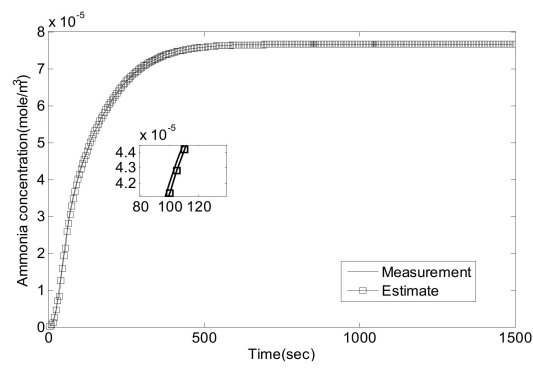


Figure 9.  $\text{NO}_2/\text{NO} = 1/2$ ,  $350\text{ }^\circ\text{C}$ , comparison of  $C_{\text{NH}_3,2}$ .

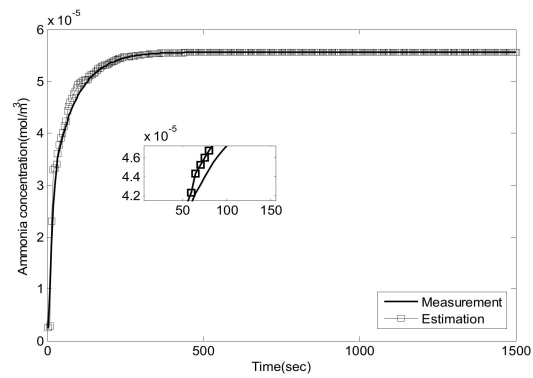


Figure 10.  $\text{NO}_2/\text{NO} = 1/2$ ,  $400\text{ }^\circ\text{C}$ , comparison of  $C_{\text{NH}_3,2}$ .

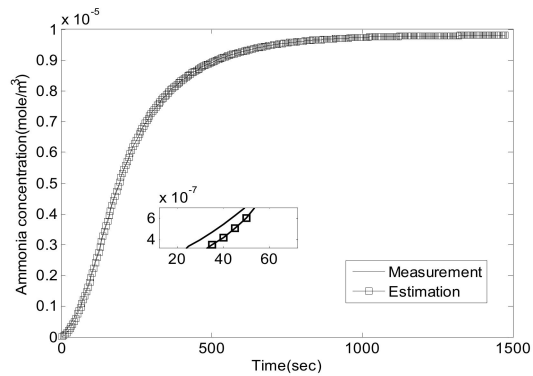


Figure 11.  $\text{NO}_2/\text{NO} = 1/1$ ,  $300\text{ }^\circ\text{C}$ , comparison of  $C_{\text{NH}_3,2}$ .

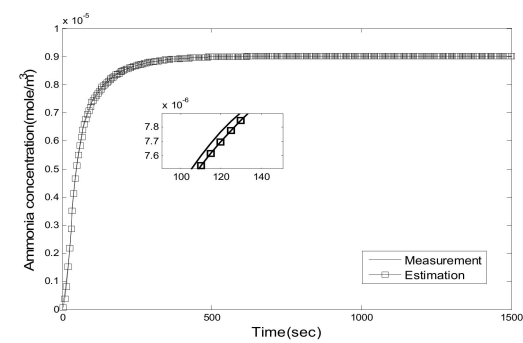


Figure 12.  $\text{NO}_2/\text{NO} = 1/1$ ,  $350\text{ }^\circ\text{C}$ , comparison of  $C_{\text{NH}_3,2}$ .

In order to show their performance more intuitively, the mean absolute error is given in Table 5.

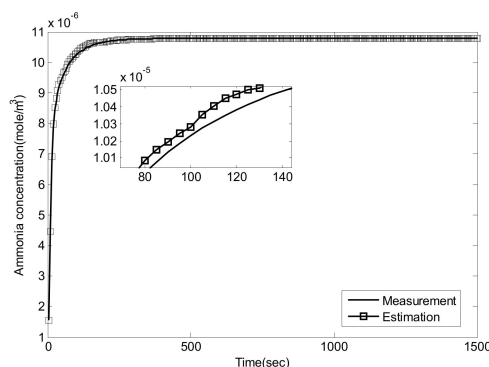


Figure 13.  $\text{NO}_2/\text{NO} = 1/1$ ,  $400^\circ\text{C}$ , comparison of  $C_{\text{NH}_3,2}$ .

Table 5. Mean absolute error for Figures 5–13.

	$\text{NO}_2/\text{NO} = 0/1$	$\text{NO}_2/\text{NO} = 1/2$	$\text{NO}_2/\text{NO} = 1/1$
$300^\circ\text{C}$	$1.9 \times 10^{-6}$	$1.6 \times 10^{-6}$	$1.1 \times 10^{-7}$
$350^\circ\text{C}$	$3.1 \times 10^{-6}$	$1.7 \times 10^{-6}$	$0.6 \times 10^{-7}$
$400^\circ\text{C}$	$4.2 \times 10^{-6}$	$2.1 \times 10^{-6}$	$1.6 \times 10^{-7}$

As can be seen, the proposed Luenberger-sliding mode observer estimation can converge to sensor measurements very well at different working conditions. The experimental results show that the observation accuracy of mid-catalyst  $\text{NH}_3$  concentration can be achieved by using the proposed observer.

## 5.2. Simulation Validation of the Luenberger-Sliding Mode Observer Based Backstepping Control for SCR System

To illustrate the validity of the Luenberger-sliding mode observer based backstepping control for the after-treatment process,  $\text{NO}_x$  conversion efficiency and  $\text{NH}_3$  leakage are taken as the output, and the injection of urea (concentration of the inlet ammonia) is taken as the input. To show the effectiveness of the proposed control strategy, traditional PID control is used for comparison. The control performance of the proposed Luenberger-sliding mode observer based backstepping control strategy is shown in Figures 14–22. The control performance of the two control methods is compared using integrated absolute error (IAE) criteria:

$$\text{IAE} = \sum |e(t)| dt \quad (73)$$

where  $e(t)$  is the error between the reference value and the actual process output. The value of IAE is enumerated in Table 6.

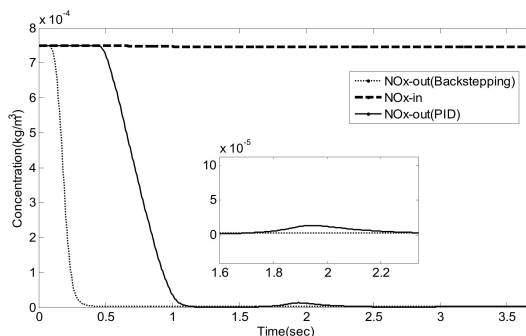


Figure 14.  $\text{NO}/\text{NO}_2 = 1/0$ ,  $\text{NO}_x$  concentration before and after the SCR system.

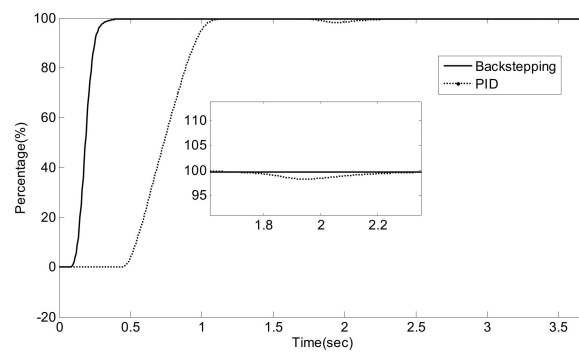


Figure 15.  $\text{NO}/\text{NO}_2 = 1/0$ ,  $\text{NO}_x$  conversion efficiency.

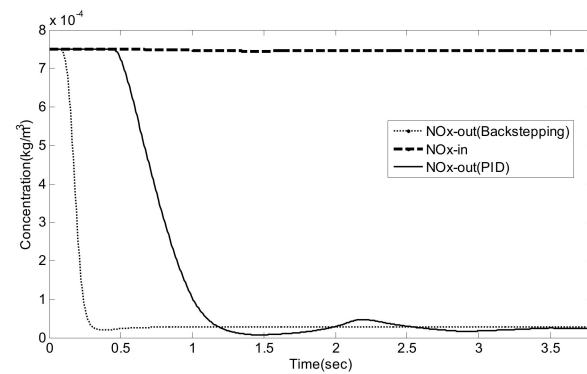


Figure 16.  $\text{NO}/\text{NO}_2 = 2/1$ ,  $\text{NO}_x$  concentration before and after the SCR system.

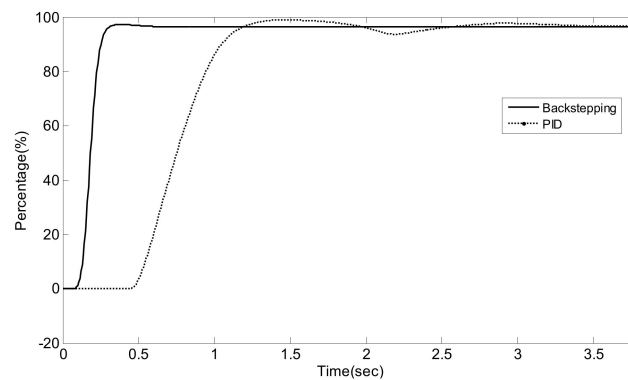


Figure 17.  $\text{NO}/\text{NO}_2 = 2/1$ ,  $\text{NO}_x$  conversion efficiency.

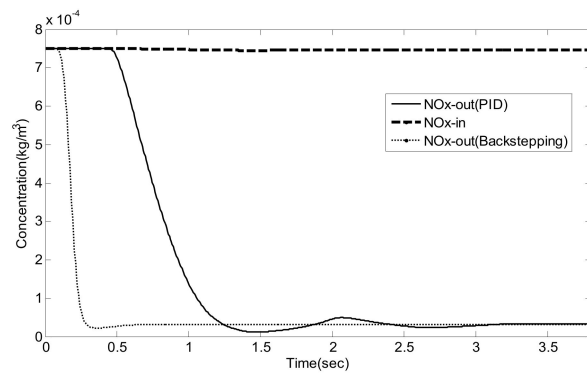


Figure 18.  $\text{NO}/\text{NO}_2 = 1/1$ ,  $\text{NO}_x$  concentration before and after the SCR system.

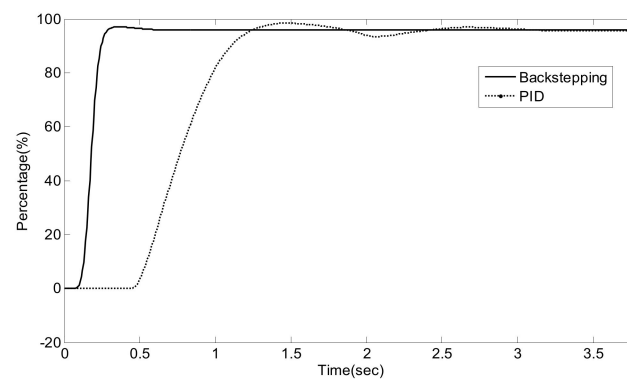


Figure 19.  $\text{NO}/\text{NO}_2 = 1/1$ ,  $\text{NO}_x$  conversion efficiency.

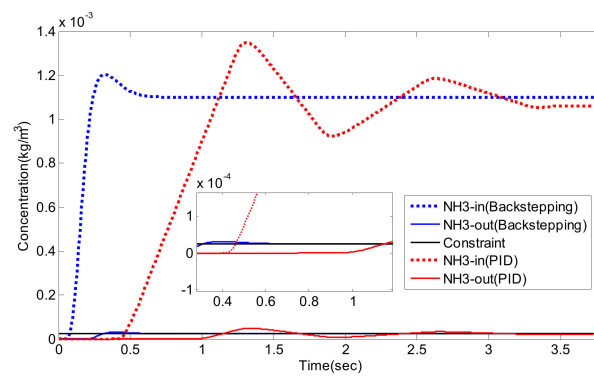


Figure 20.  $\text{NO}/\text{NO}_2 = 1/0$ ,  $\text{NH}_3$  concentration before and after the SCR system.

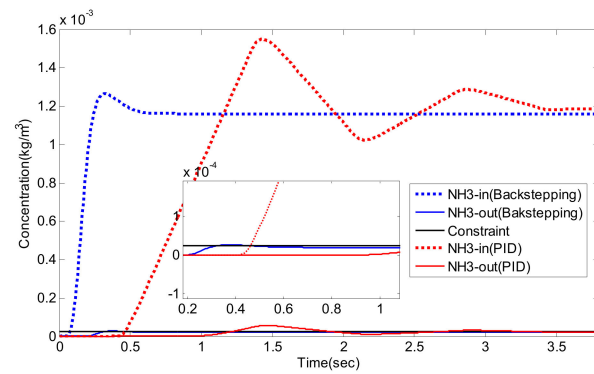


Figure 21.  $\text{NO}/\text{NO}_2 = 2/1$ ,  $\text{NH}_3$  concentration before and after the SCR system.

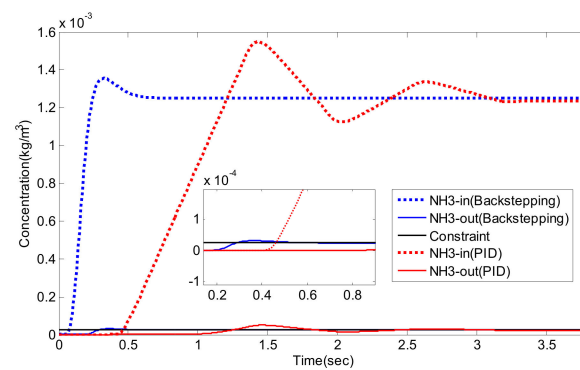


Figure 22.  $\text{NO}/\text{NO}_2 = 1/1$ ,  $\text{NH}_3$  concentration before and after the SCR system.

**Table 6.** Control performance of the two control strategies.

	NO/NO <sub>2</sub>	Settling Time (s)	Overshoot (%)	Integrated Absolute Error (IAE)
PID	1/0	3.2	27.8	0.1482
	2/1	3.3	30.0	0.1784
	1/1	3.1	25.2	0.1649
Luenberger-Sliding Mode Observer Based Backstepping	1/0	0.49	9.3	0.0373
	2/1	0.49	8.9	0.0295
	1/1	0.48	8.3	0.0310

As can be seen from Figures 14–22 and Table 6, traditional PID control and Luenberger-sliding mode observer based backstepping control can basically meet the control requirements, and both can achieve high NO<sub>x</sub> conversion rate when the NH<sub>3</sub> leakage in the tail gas exceeds the standard, or when a small amount exceeds the standard. Nevertheless, traditional PID control has a large overshoot, which is when it injects excessive adblue into the engine exhaust in a short time. As can be seen from Figure 14, Figures 16 and 19, NH<sub>3</sub> emission from the SCR catalytic converter outlet fluctuates for a period of time, which does not meet the requirements of emission regulations. The proposed controller reaches better operating points in which about 96.2% of NO<sub>x</sub> is reduced while allowing about 24 ppm NH<sub>3</sub> slip past the catalyst. Although the backstepping control method also has a small amount of overshoot, the downstream emission of the SCR catalysts does not exceed the limit, which is in line with the requirements of emission regulations. Moreover, the backstepping control method has a shorter adjustment time. Even in the case of overshoot, NH<sub>3</sub> emissions downstream of the SCR catalyst can quickly return to normal levels, which is conducive to achieving a higher NO<sub>x</sub> conversion rate. Furthermore, the control response obtained using the Luenberger-sliding mode observer based backstepping controller has smaller overshoot and relatively shorter settling time. The control responses indicate the efficiency of the proposed controller with excellent set-point tracking properties.

## 6. Conclusions

In this paper, a Luenberger-sliding mode observer based backstepping control strategy was proposed to estimate the mid-catalyst ammonia concentration and calculate the input of adblue. The dynamics of a SCR system was modeled to represent the actual process in the design study of the Luenberger-sliding mode observer based backstepping control strategy. The Lyapunov technique was used for demonstrating the stability of the observer and the backstepping SCR control method. Through the simulation test, the performance of the Luenberger-sliding mode observer and the proposed approach was verified under the conditions of different intake components and different intake temperatures. The results show that the observer has high estimation accuracy under different conditions, with a maximum average error of less than  $4.2 \times 10^{-6}$ . Furthermore, the Luenberger-sliding mode observer based backstepping control strategy can keep the ammonia slip of the downstream SCR system at a low level and simultaneously achieve a high NO<sub>x</sub> conversion rate, which is much better than the popular PID control method in setting time, overshoot, and tracking error.

**Author Contributions:** Conceptualization, T.Z.; Methodology, Y.L.; Software, B.Y.; Validation, Y.M.; formal analysis, Y.M.; Investigation, T.Z.; Resources, B.Y.; Data curation, B.Y.; Writing, T.Z.; Writing—review and editing, Y.M.

**Funding:** This research was funded by the Foundation and Frontier Projects in Chongqing, grant number cstc2018jcyjAX0684.

**Conflicts of Interest:** The authors declare no conflict of interest.

## References

1. Christoph, M.S.; Christopher, H.O.; Hans, P.G. Control of an SCR catalytic converter system for a mobile heavy-duty application. *IEEE Trans. Control Syst. Technol.* **2006**, *14*, 641–653.

2. Yan, F.; Wang, J. Control of diesel engine dual-loop EGR air-path systems by a singular perturbation method. *Control Eng. Pract.* **2013**, *21*, 981–988. [\[CrossRef\]](#)
3. Lee, S.; Park, S. Numerical analysis of internal flow characteristics of urea injectors for SCR dosing system. *Fuel* **2014**, *129*, 54–60. [\[CrossRef\]](#)
4. Chen, P.; Wang, J. A novel cost-effective robust approach for selective catalytic reduction state estimations using dual nitrogen oxide sensors. *J. Automot. Eng.* **2015**, *229*, 83–96. [\[CrossRef\]](#)
5. Devarakonda, M.; Parker, G.; Johnson, J.H.; Strots, V. Model-based control system design in a urea-SCR aftertreatment system based on  $\text{NH}_3$  sensor feedback. *Int. J. Automot. Technol.* **2009**, *10*, 653–662. [\[CrossRef\]](#)
6. Yan, F.; Wang, J. Design and robustness analysis of discrete observers for diesel engine in-cylinder oxygen mass fraction cycle-by-cycle estimation. *Control Syst. Technol.* **2012**, *20*, 72–83.
7. Ham, Y.; Park, S. Development of Map based Open Loop Control Algorithm for Urea-SCR System. *Trans. Korean Soc. Automot. Eng.* **2011**, *19*, 50–56.
8. Zhang, S.M.; Tian, F.; Ren, G.F.; Yang, L.S. CR control strategy based on ANNs and Fuzzy PID in a heavy-duty diesel engine. *Int. J. Automot. Technol.* **2012**, *13*, 693–699. [\[CrossRef\]](#)
9. Kim, Y.; Park, T.; Jung, C. Hybrid Nonlinear Model Predictive Control of LNT and Urealess SCR Aftertreatment System. *IEEE Trans. Control Syst. Technol.* **2019**, *27*, 2305–2313. [\[CrossRef\]](#)
10. Zhao, J.H.; Hu, Y.F.; Gong, X.; Chen, H. Modelling and control of urea-SCR systems through the triple-step non-linear method in consideration of time-varying parameters and reference dynamics. *Trans. Inst. Meas. Control* **2018**, *40*, 287–302. [\[CrossRef\]](#)
11. Yang, B.; Keqiang, L.; Ukawa, H.; Handa, M. Modelling and control of a non-linear dynamic system for heavy-duty trucks. *Proc. Inst. Mech. Eng. Part D J. Automot. Eng.* **2006**, *220*, 1423–1435. [\[CrossRef\]](#)
12. Chang, Y.H.; Chan, W.S.; Chang, C.W. T-S fuzzy model-based adaptive dynamic surface control for ball and beam system. *IEEE Trans. Ind. Electron.* **2013**, *60*, 2251–2263. [\[CrossRef\]](#)
13. Chi, J.N.; DaCosta, H.F.M. Modeling and control of a urea-SCR aftertreatment system. *SAE Trans.* **2005**, *114*, 449–465.
14. Devarakonda, M.; Parker, G.; Johnson, J.H. Model-based estimation and control system development in a urea-SCR aftertreatment system. *SAE Int. J. Fuels Lubr.* **2009**, *1*, 646–661. [\[CrossRef\]](#)
15. Liu, Q.F.; Chen, H.; Hu, Y.F.; Sun, P.Y.; Li, J. Modeling and control of the fuel injection system for rail pressure regulation in GDI engine. *IEEE/ASME Trans. Mechatron.* **2014**, *19*, 1501–1513.
16. Westerlund, C.; Westerberg, B.; Ingemar, O.; Egnell, R. Model predictive control of a combined EGR/SCR HD diesel engine[C]. *SAE2010 World Congr. Exhib.* **2010**, 13–15. [\[CrossRef\]](#)
17. Ebrahimian, V.; Habchi, C.; Nicolle, A. Detailed modeling of the evaporation and thermal decomposition of urea-water solution in SCR systems. *AIChE J.* **2012**, *58*, 1998–2009. [\[CrossRef\]](#)
18. Chen, P.; Wang, J. Observer-based estimation of air-fractions for a diesel engine coupled with aftertreatment systems. *Control Syst. Technol.* **2013**, *21*, 2239–2250. [\[CrossRef\]](#)
19. Bonfils, A.; Creff, Y.; Lepreux, O.; Petit, N. Closed-loop control of a SCR system using a  $\text{NO}_x$  sensor cross-sensitive to  $\text{NH}_3$ . *J. Process Control* **2014**, *24*, 368–378. [\[CrossRef\]](#)
20. Davila, J.; Fridman, L.; Levant, A. Second-Order Sliding-Mode-observer for Mechanical Systems. *IEEE Trans. Autom. Control* **2005**, *50*, 1785–1789. [\[CrossRef\]](#)
21. Foo, G.; Rahman, M.F. Sensorless sliding-mode MTPA control of an IPM synchronous motor drive using a sliding-mode observer and HF signal injection. *IEEE Trans. Ind. Electron.* **2010**, *57*, 1270–1278. [\[CrossRef\]](#)
22. Kubinski, D.J.; Visser, J.H. Sensor and method for determining the ammonia loading of a zeolite SCR catalyst. *Sens. Actuators B Chem.* **2008**, *130*, 425–429. [\[CrossRef\]](#)
23. Hsieh, M.; Wang, J. Sliding-mode observer for urea-selective catalytic reduction (SCR) mid-catalyst ammonia concentration estimation. *Int. J. Automot. Technol.* **2011**, *12*, 321–329. [\[CrossRef\]](#)
24. Hasan, S.N.; Husain, I. A Luenberger-sliding mode observer for online parameter estimation and adaptation in high-performance induction motor drives. *IEEE Trans. Ind. Appl.* **2009**, *45*, 772–781. [\[CrossRef\]](#)
25. Sun, W.C.; Gao, H.J.; Kaynak, O. Adaptive backstepping control for active suspension systems with hard constraints. *IEEE/ASME Trans. Mechatron.* **2013**, *18*, 1072–1079. [\[CrossRef\]](#)
26. Hamida, A.; Leon, J.; Glumineau, A. Experimental sensorless control for IPMSM by using integral backstepping strategy and adaptive high gain observer. *Control Eng. Pract.* **2017**, *59*, 64–76. [\[CrossRef\]](#)
27. Hsieh, M.; Wang, J. A two-cell backstepping-based control strategy for diesel engine selective catalytic reduction systems. *Control Syst. Technol.* **2014**, *24*, 1504–1515. [\[CrossRef\]](#)

28. Olsson, L.; Sjövall, H.; Blint, R.J. A kinetic model for ammonia selective catalytic reduction over Cu-ZSM-5. *Appl. Catal. B Environ.* **2008**, *81*, 203–217. [\[CrossRef\]](#)
29. Zheng, T.; Han, W.; Li, Y.; Yang, B.; Shi, L. Luenberger-sliding modeobserver based ammonia concentration estimation for selectivecatalyst reduction system[C]. In Proceedings of the 2016 12th World Congress on Intelligent Control and Automation (WCICA), Guilin, China, 12–15 June 2016; pp. 3021–3026.
30. Morandi, S.; Prinetto, F.; Ghiotti, G.; Castoldi, L.; Lietti, L.; Forzatti, P.; Daturi, M.; Blasin-Aubé, V. The influence of CO<sub>2</sub> and H<sub>2</sub>O on the storage properties of Pt-Ba/Al<sub>2</sub>O<sub>3</sub> LNT catalyst studied by FT-IR spectroscopy and transient microreactor experiments. *Catal. Today* **2014**, *231*, 116–124. [\[CrossRef\]](#)
31. Shimizu, K.; Satsuma, A. Hydrogen assisted urea-SCR and NH<sub>3</sub>-SCR with silver–alumina as highly active and SO<sub>2</sub>-tolerant de-NO<sub>x</sub> catalysis. *Appl. Catal. B Environ.* **2007**, *77*, 202–205. [\[CrossRef\]](#)
32. Doronkin, D.E.; Fogel, S.; Tamm, S.; Olsson, L.; Khan, T.S.; Bligaard, T.; Gabrielsson, P.; Dahl, S. Study of the “Fast SCR”-like mechanism of H<sub>2</sub>-assisted SCR of NO<sub>x</sub> with ammonia over Ag/Al<sub>2</sub>O<sub>3</sub>. *Appl. Catal. B Environ.* **2012**, *113*, 228–236. [\[CrossRef\]](#)



© 2019 by the authors. Licensee MDPI, Basel, Switzerland. This article is an open access article distributed under the terms and conditions of the Creative Commons Attribution (CC BY) license (<http://creativecommons.org/licenses/by/4.0/>).